NeuroImage: Clinical 50 (2026) 104002

Contents lists available at ScienceDirect

NeuroImage: Clinical

journal homepage: www.elsevier.com/locate/ynicl

Functional gradient reorganization and transcriptomic signatures underlying 1 Hz rTMS treatment in first-episode schizophrenia following right orbitofrontal cortex stimulation

Wenwen Miao [a,1], Xiong Jiao [b,1], Ningning Zeng [a,c], Min Wang [d], Kexu Zhang [e], Cheng Yang [b], Yuanjun Xie [f,*], Ziliang Wang [g,*], Qiang Hu [a,*]

[a] Department of Psychiatry, Wuhu Hospital of Anding Hospital (The Fourth People's Hospital of Wuhu), Wuhu 241000, China
[b] Shanghai Key Laboratory of Psychotic Disorders, Shanghai Mental Health Center, Shanghai JiaoTong University School of Medicine, Shanghai 200030, China
[c] Cognitive Neuroscience Center, University Medical Center Groningen, Groningen, The Netherlands
[d] Department of Psychology, School of Humanities and Social Sciences, University of Science and Technology of China, Hefei 230026, China
[e] Department of Psychiatry, Shandong Daizhuang Hospital, Jining 272051, China
[f] School of Medicine, Sichuan University of Science and Engineering, Zigong 643000, China
[g] Department of Psychiatry, Zhenjiang Mental Health Center, Zhenjiang 212000, China

ARTICLE INFO

Keywords:
Schizophrenia
Transcranial magnetic stimulation
Orbitofrontal cortex
Functional gradient
Imaging transcriptomics

ABSTRACT

Background: The orbitofrontal cortex (OFC) represents a promising yet underexplored neuromodulation target for negative symptoms in schizophrenia, and the macroscale and microscale mechanisms underlying its therapeutic effects remain unclear.

Methods: In a randomized, double-blind, sham-controlled trial, 84 patients with drug-naïve first-episode schizophrenia received consecutive 20 days of active 1-Hz repetitive transcranial magnetic stimulation (rTMS) over the right OFC (n = 45) or sham (n = 39). Resting-state fMRI gradient mapping was integrated with imaging transcriptomics to characterize multiscale neural reorganization and predict treatment response.

Results: Active rTMS was associated with greater improvement in negative symptoms and general psychopathology compared with sham stimulation. Gradient analyses indicated a renormalization of macroscale functional hierarchy, with increased principal gradient scores in transmodal nodes (e.g., right middle occipital gyrus and angular gyri) and decreased scores in salience-related regions (e.g., anterior cingulate cortex). These spatial patterns were coupled to transcriptomic signatures enriched for synaptic plasticity and ion transport, with cell-type enrichment implicating cortical interneurons and oligodendrocytes. In addition, baseline gradient topographies in the right middle occipital gyrus and ventral attention network predicted improvements in negative and general symptoms, respectively.

Conclusions: Low-frequency OFC-rTMS was associated with alleviation of negative symptoms in first-episode schizophrenia, alongside a reconfiguration of cortical functional hierarchy. The observed gradient effects were spatially linked to molecular pathways underlying synaptic plasticity and excitation–inhibition regulation, supporting functional gradients as biomarkers for precision neuromodulation in early-stage schizophrenia.

1. Introduction

Schizophrenia is a debilitating psychiatric disorder characterized by a constellation of perceptual, cognitive, and behavioral impairments, among which negative symptoms and cognitive dysfunction are particularly refractory to conventional pharmacological intervention (Miyamoto et al., 2012; Siever Larry and Davis Kenneth, 2004). While repetitive transcranial magnetic stimulation (rTMS) has emerged as a safe and promising neuromodulatory approach (Blyth et al., 2025), clinical outcomes targeting conventional targets, such as the dorsolateral prefrontal cortex (DLPFC) and temporoparietal cortex (TPC), remain highly heterogeneous (Freitas et al., 2009; He et al., 2017; Yi

* Corresponding authors.
E-mail addresses: xieyuanj@gmail.com (Y. Xie), wangziliang201@163.com (Z. Wang), huqiang0704@163.com (Q. Hu).
[1] These authors are regarded as co-first authors.

https://doi.org/10.1016/j.nicl.2026.104002
Received 23 February 2026; Received in revised form 20 April 2026; Accepted 3 May 2026
Available online 5 May 2026

et al., 2024). Consequently, recent research has shifted toward the orbitofrontal cortex (OFC) (Robin and Bastin, 2025), a critical hub for emotion regulation, reward processing, and decision-making (Rolls, 2023; Rolls et al., 2020; Rudebeck and Rich, 2018). Structural and functional abnormalities within the OFC, including altered cortical thickness, white matter connections, and diminished striatal coupling, have been closely associated with the severity of negative symptoms in schizophrenia (Ohtani et al., 2014; Shukla et al., 2019a; Walton et al., 2018). Building on this evidence, our recent randomized, double-blind, sham-controlled trial demonstrated that 1-Hz rTMS applied to the right OFC produced significant improvements in negative symptoms and cognitive performance in drug-naïve patients with first-episode schizophrenia (Hu et al., 2023). Despite these encouraging clinical results, the system-level network mechanisms mediating recovery and the molecular substrates underlying rTMS-induced plasticity remain to be elucidated.

To elucidate how focal stimulation of the OFC propagates to reorganize large-scale brain function, it is essential to move beyond assessments of local activity and interrogate the topological architecture of the cortex. Recent advances in connectomic have reconceptualized cortical organization as a continuous functional gradient that spanning from unimodal sensorimotor territories to transmodal association areas (Huntenburg et al., 2018; Margulies et al., 2016). In schizophrenia, this macroscale hierarchy is frequently compressed from the sensorimotor region (Dong et al., 2023; Uslu et al., 2025), reflecting a fundamental failure to integrate incoming sensory information with higher-order cognitive processes, a phenomenon often described as a dysconnection syndrome (Friston, 1999). Because the OFC occupies a distinct position within this hierarchical gradient, targeted modulation of OFC activity with rTMS has the potential to induce widespread reorganization of the principal functional gradient. To date, however, few studies have directly investigated whether the clinical benefits of OFC-directed rTMS are mediated by restoration of these global cortical gradients, particularly in the early stages of the illness where neural plasticity and network malleability are most critical.

Macroscale reorganization is ultimately grounded in microscale molecular processes, particularly those governing synaptic plasticity and excitation-inhibition balance. While direct in vivo visualization of these molecular landscapes remains challenging in humans, imaging transcriptomics provides a robust framework to bridge this gap by linking macroscopic neuroimaging phenotypes with high-resolution gene expression profiles from the Allen Human Brain Atlas (AHBA) (Shen et al., 2012). Emerging evidence indicates that the spatial topography of functional gradients is tightly coupled with the expression profiles of genes enriched for synaptic signaling and neuronal development in schizophrenia (Xiang et al., 2025). Specifically, in patients with drug-naïve first-episode schizophrenia, dysfunction in the principal functional gradient has been shown to spatially covary with transcriptional signatures related to specific cell types and signaling pathways, which in turn hold predictive value for treatment response (Yao et al., 2024). By applying this approach to map rTMS-induced gradient alterations against transcriptomic atlases, it becomes possible to identify the specific biological mechanisms that facilitate network recovery following neuromodulation.

In the present study, resting-state fMRI data from a prior randomized controlled trial was leveraged to elucidate the multiscale mechanisms of 1-Hz OFC-rTMS in drug-naïve, first-episode schizophrenia. A high-resolution parcellation (Schaefer 400) (Schaefer et al., 2018) was employed to calculate the principal functional gradient, and treatment-related reorganization was quantified at the global, subnetwork, and nodal levels (Xie et al., 2024). Partial least squares (PLS) regression was then utilized to link these gradient alterations to spatial gene expression profiles (Datta, 2018), followed by comprehensive enrichment analyses spanning functional pathways, cognitive terms, and Context-Specific Expression Analysis (CSEA) (Dougherty et al., 2010). It was hypothesized that: (1) normalization of the principal cortical gradient, particularly within transmodal networks, would be induced by active rTMS; (2) this reorganization would be spatially associated with the expression of genes enriched for synaptic plasticity and neurotransmission; and (3) baseline gradient topography would be identified as a predictive biomarker for clinical improvement.

2. Materials and methods

2.1. Participants

This study was designed as a randomized, double-blind, sham-controlled clinical trial (Hu et al., 2023). Patients with first-episode schizophrenia were recruited from the Department of Psychiatry at the First Psychiatric Hospital of Harbin. A total of 98 patients were initially recruited and randomly assigned to either the active rTMS group or the sham rTMS group. After accounting for dropouts due to incomplete assessments, the final sample consisted of 89 patients: 47 in the active rTMS group and 42 in the sham rTMS group. For the present neuroimaging analysis, five additional patients were excluded because of excessive head motion, resulting in a final sample of 84 patients, including 45 in the active rTMS group and 39 in the sham group. The inclusion criteria were as follows: (1) a diagnosis of schizophrenia according to DSM-5 criteria; (2) age between 15 and 45 years; (3) an intelligence quotient (IQ) $>$ 69; (4) rug-naïve and experiencing their first episode of psychosis; (5) a Positive and Negative Syndrome Scale (PANSS) total score $\geq$ 60; and (6) a Clinical Global Impression (CGI) score $\geq$ 4. After enrollment, patients received atypical antipsychotic treatment. In the parent neuroimaging sample, 40 patients in the active rTMS group and 36 in the sham group were treated with olanzapine, whereas 5 and 3 patients, respectively, received aripiprazole; the prescribed dose range was 10-15 mg per day, with sedatives such as alprazolam and zolpidem tartrate used as needed. There was no significant between-group difference in antipsychotic medication type ($\chi^2 = 0.283$, $p = 0.594$). Exclusion criteria included sensorimotor disorders, neurological diseases (e.g., epilepsy), metal implants contraindicating MRI/TMS, history of electroconvulsive therapy (ECT) within the past month, substance abuse, or pregnancy. Participants were assigned to groups using computer-generated randomization by an independent third party. Both patients and clinical raters were blinded to the treatment allocation.

The study protocol was approved by the Research Ethics Committee of the First Psychiatric Hospital of Harbin and was registered with the Chinese Clinical Trial Register (ChiCTR2000041106). Written informed consent was obtained from all participants prior to enrollment.

2.2. Clinical assessments

The primary clinical outcome was assessed using the Positive and Negative Syndrome Scale (PANSS) (Kay et al., 1987), which includes positive, negative, and general psychopathology to capture a comprehensive profile of symptom dimensions. Secondary outcomes regarding overall functional and illness severity, evaluated using the Global Assessment of Functioning (GAF) scale (Endicott et al., 1976) and the Clinical Global Impressions (CGI) scale (Forkmann et al., 2011), respectively. Symptom severity and global functioning were evaluated by experienced psychiatrists who were blinded to treatment allocation. Clinical measurements were administered at two points: baseline and immediately upon completion of the intervention. The inter-rater reliability for the clinical assessments was 0.86, indicating good consistency across raters.

2.3. rTMS protocol

rTMS was delivered using a MagPro X100 stimulator (Medtronic, Denmark) equipped with a butterfly coil (Cool D-B80). In the active group, the coil was positioned over the OFC, corresponding to the AF8

electrode location in the international 10-10 EEG system. Stimulation was applied at 1 Hz and intensity of 110% of the resting motor threshold (RMT). RMT was determined over the primary motor cortex using a visual method, with the contralateral abductor pollicis brevis (APB) serving as the target muscle. Stimulation intensity was adjusted in 1% - 2% increments, and the threshold was defined as the minimum intensity that elicited a clearly visible contraction of the APB in at least 5 of 10 consecutive trials. Treatment was administered once daily for 20 consecutive days. Each session consisted of 12 trains of 60 s, separated by 30-second inter-train intervals, for a total of 720 pulses per session. Although this motor-threshold-based dosing approach is widely used in clinical rTMS studies, it does not fully account for anatomical and excitability differences between the motor cortex and the OFC. Without target-specific dose adjustment or electric field modeling, the effective cortical dose delivered to the OFC may therefore have varied across participants. In the sham group, the same coil, target location, and stimulation schedule were used, but the coil was flipped 180° to reduce effective brain stimulation while preserving the general acoustic artifact and part of the scalp sensation associated with active stimulation. It should be noted that this sham procedure may not represent a fully inert placebo condition and may not completely reproduce the somatosensory features of active OFC stimulation.

2.4. MRI data acquisition

Magnetic resonance imaging (MRI) data were acquired using a 3.0-Tesla GE Discovery MR750 scanner equipped with a 32-channel head coil. Resting-state functional MRI (fMRI) images were obtained using an echo-planar imaging (EPI) sequence with the following parameters: repetition time (TR) = 2000 ms; echo time (TE) = 45 ms; flip angle (FA) = 90°; field of view (FOV) = 256 x 256 mm; matrix size = 64 x 64; slice thickness = 4 mm, voxel size = 3.125 mm x 3.125 mm x 4.5 mm, 180 volumes. Anatomical T1-weight images were acquired using a 3D fast gradient echo sequence following the parameters: TR = 8.20 ms, TE = 3.22 ms, FA = 12°, FOV = 256 x 256 mm, matrix size = 512 x 512, slice thickness = 1 mm, 184 slices. During scanning, participants were instructed to keep their eyes closed, stay awake, and minimize head movement.

2.5. fMRI preprocessing

Preprocessing of resting-sate fMRI data was performed using standard DPABI toolbox pipelines (https://rfmri.org/DPABI) implemented on the SPM12 platform (https://www.fil.ion.ucl.ac.uk/spm). The preprocessing steps included: (1) removal of the first 10 time points to allow for signal equilibrium; (2) slice timing correction; (3) realignment for head motion correction; (4) co-registration of the functional images to T1-weighted structural image; (5) segmentation of the T1-weighted image into gray matter, white matter, and cerebrospinal fluid tissue probability maps; (6) spatial normalization to Montreal Neurological Institute (MNI) space using the DARTEL algorithm, with images resampled to 3-mm isotropic voxels; (7) nuisance regression including the Friston-24 head motion parameters, white matter signal, cerebrospinal fluid signal, and global signal; (8) spatial smoothing with a 6-mm full width at half maximum (FWHM) Gaussian kernel; and (9) temporal band-pass filtering was applied (0.01–0.1 Hz). Global signal regression was included to reduce widespread non-neuronal variance and motion-related global artifacts, thereby improving the specificity of functional connectivity estimates, although it is recognized that this preprocessing choice remains methodologically debated (Ciric et al., 2017; Murphy and Fox, 2017). Head motion was quantified using mean framewise displacement (FD) according to the method of Power et al (Power et al., 2012). Participants with mean FD > 0.3 mm were excluded from further analysis. The preprocessed functional data were then parcellated into 400 cortical regions of interest (ROIs) using the Schaefer 400-parcellation atlas, which assigns parcels to the seven canonical Yeo networks (Visual, Somatomotor, Dorsal Attention, Ventral Attention, Limbic, Frontoparietal, and Default Mode) (Thomas Yeo et al., 2011).

2.6. Functional gradient analysis

The BrainSpace toolbox (Vos de Wael et al., 2020) was used to estimate the principal functional gradient. For each participant, a 400 x 400 functional connectivity matrix was first constructed using Pearson correlation. To reduce the contribution of weak and potentially noisy connections while preserving the dominant large-scale topological structure of the connectome, each matrix was thresholded to retain the top 10% of connections. The thresholded matrix was subsequently transformed into an affinity matrix using cosine similarity (kernel = cosine), which quantifies the similarity of connectivity profiles between cortical regions and is commonly used in connectome gradient studies. Laplacian eigenmaps (approach = le) were subsequently applied to decompose the affinity matrix into manifold components (gradients). This nonlinear embedding approach was selected because it provides a robust representation of continuous macroscale cortical organization and has been widely adopted in prior gradient-mapping studies (Hong et al., 2020). Although no single threshold or kernel is universally optimal, the present parameter settings were chosen to align with commonly used practices in connectome gradient analysis and to balance noise suppression with preservation of meaningful large-scale connectivity structure (Margulies et al., 2016). Analyses were then focused on the principal gradient (Gradient 1), which explains the largest variance in the connectivity data and captures the primary axis of macroscale cortical organization.

To ensure topographical comparability across individuals and time points, individual gradient maps were aligned to a group-level template constructed from the baseline data using Procrustes Alignment. Four complementary metrics were computed to characterize gradient topography: (1) gradient scores, defined as the value of each node along the principal gradient axis; (2) gradient range, defined as the difference between the maximum and minimum gradient scores, indexing the expansion or compression of the functional hierarchy; (3) gradient variance, indicating the variability of gradient scores across the cortex; and (4) explained ratio, defined as the proportion of the total connectome variance accounted for by the principal gradient.

Statistical comparisons were conducted at multiple spatial scales, including the global level (range and variance), subnetwork level (mean gradient scores within each of the seven canonical networks), and nodal level, to evaluate effects of group (rTMS vs. Sham) and time (Base vs. Post). The significance threshold was set at $p < 0.05$. Multiple comparisons were controlled using false discovery rate (FDR) correction for subnetwork- and nodal-level analyses, as appropriate. Age, sex, and years of education were included as covariates in all relevant models.

2.7. Imaging transcriptomics

To investigate the molecular substrates underlying rTMS-induced gradient reorganization, microarray gene expression data from the AHBA were leveraged. AHBA data were preprocessed using the abagen toolbox following standardizing workflows (Markello et al., 2021). Probes were reannotated, and expression values were normalized and mapped to the Schaefer 400 parcellation scheme. To ensure robustness, only genes demonstrating high differential stability (> 0.5) across donors were retained for subsequent analyses. Partial Least Squares (PLS) regression was then performed to identify genes whose spatial expression patterns covaried with the cortical map of rTMS-induced gradient changes. The statistical significance of the PLS components was assessed using permutation testing. To account for spatial autocorrelation intrinsic to both neuroimaging and transcriptomic data, spin-permutation tests were additionally applied to generate spatially constrained null models. Genes were considered significant if they survived FDR correction ($p < 0.05$). From the resulting gene set, genes

contributing most strongly to the spatial association were selected for downstream enrichment analyses using a stringent threshold on normalized PLS weights ($Z > 5$ or $Z < -5$).

2.8. Functional decoding and cell type enrichment

Cognitive decoding was performed using the Neurosynth database (https://neurosynth.org), enabling quantitative associations between the identified gradient maps and meta-analytic cognitive terms (e.g., "memory," "executive function"). To further delineate the cellular substrates of these gene signatures, CSEA was conducted using the CSEA web tool (https://doughertytools.wustl.edu/CSEAtool.html). The significant gene list derived from the PLS analysis was input into the CSEA to test enrichment across specific cell types and across human developmental stages and adult brain regions. Statistical significance of cell-type enrichment was evaluated using Fisher's exact test with FDR correction ($p < 0.05$).

2.9. Prediction analysis

A unified PLS regression framework was employed to examine whether baseline functional hierarchy moderates therapeutic responses. For each clinical outcome (PANSS subscale), the response variable was defined as the longitudinal score change (Post - Pre). The predictor matrix comprised standardized baseline gradient features, at either the nodal or subnetwork levels, together with their interaction terms with treatment assignment (Baseline x Group). Model complexity was optimized using 5-fold cross-validation, and predictive performance was quantified by the coefficient of determination (R^2). Statistical significance of the overall model was assessed using permutation testing with 300 iterations. PLS weights and variable Importance in Projection (VIP) scores were further computed to identify gradient features contributing most strongly to the interaction effects; features with VIP scores > 1.0 and $p < 0.05$ were interpreted as putative moderators of rTMS efficacy. These analytic procedures were selected in accordance with commonly used resampling and feature-importance strategies in PLS-based neuroimaging analyses (Farrés et al., 2015; Krishnan et al., 2011). Given the moderate sample size and the absence of a fully nested validation framework, these predictive analyses should be regarded as exploratory and interpreted with appropriate caution. An overview of the experimental design, data processing, and analytical pipeline is illustrated in Fig. 1.

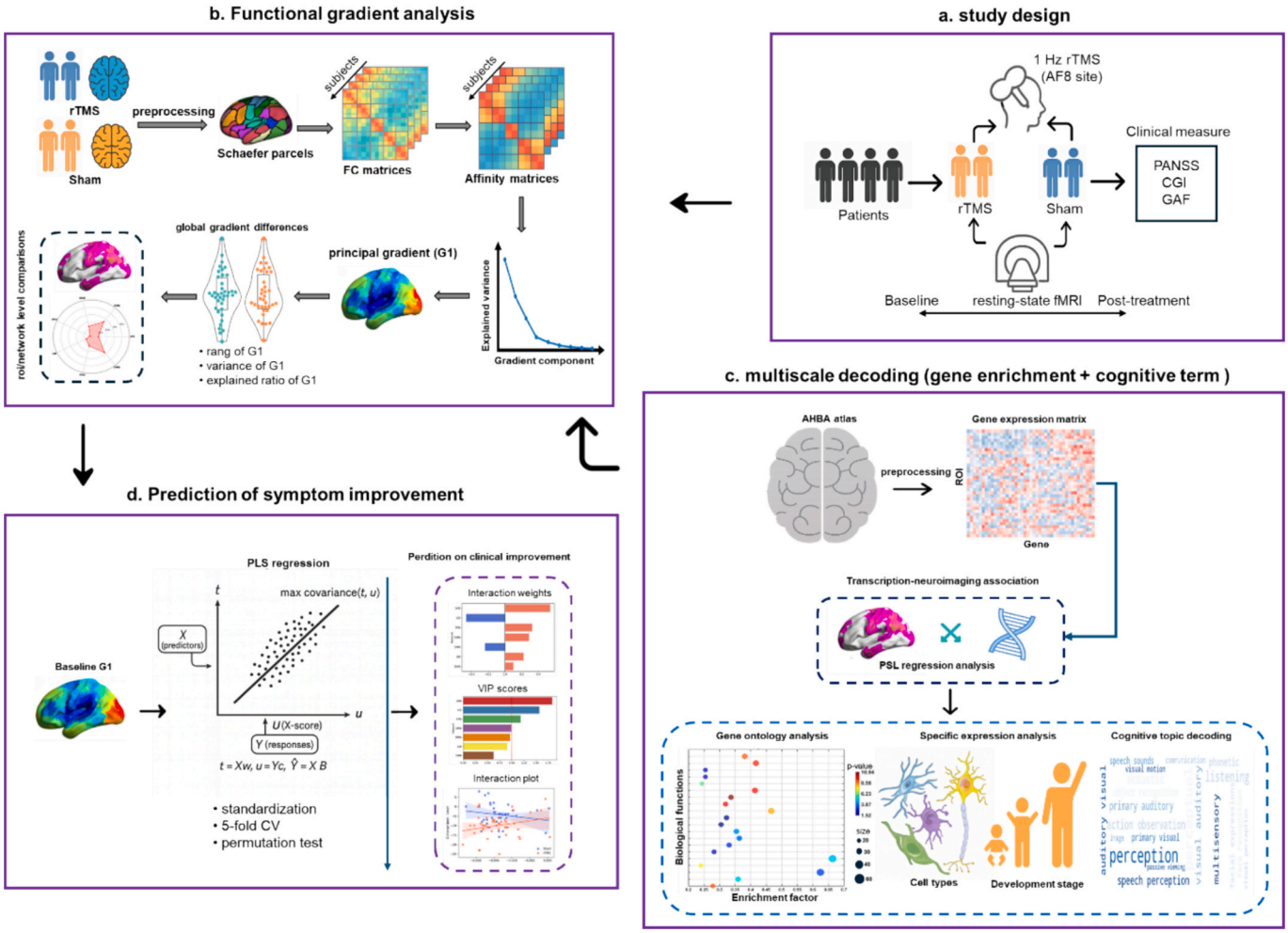

Fig. 1. Schematic overview of the study design and analytical pipeline. (a) Study Design: Drug-naïve patients with first-episode schizophrenia were randomized to receive 20 sessions of active 1-Hz rTMS (target: right OFC) or sham stimulation. Clinical and fMRI data were acquired at baseline and post-treatment. (b) Functional Gradient Analysis: The principal functional gradient (G1) was computed based on the Schaefer-400 parcellation using diffusion map embedding. rTMS-induced gradient alterations were assessed at global, subnetwork, and nodal levels. (c) Multiscale Decoding: An imaging transcriptomics approach linked gradient changes to gene expression profiles from the Allen Human Brain Atlas (AHBA). Significant genes identified via PLS regression were decoded for functional enrichment (GO), cell-type specificity (SEA), and cognitive associations (Neurosynth). (d) Prediction Analysis: A unified PLS regression model incorporating baseline gradient features and their interaction with treatment (Baseline x Group) was employed to predict clinical symptom improvement.

3. Results

3.1. Demographic and clinical Characteristics

Five patients were excluded due to excessive head motion (FD > 0.3) and imaging artifacts (rTMS group: n = 2; Sham group: n = 3). Accordingly, 84 patients with first-episode schizophrenia were included in the final neuroimaging analysis, consisting of 45 in the active rTMS group and 39 in the sham group. As summarized in Table 1, no significant between-group differences were observed in age (t = 0.400, p = 0.690), sex distribution (χ^2 = 0.671, p = 0.413), years of education (t = 1.032, p = 0.305), or duration of untreated psychosis (DUP) (t = 0.930, p = 0.355).

3.2. Clinical treatment outcomes

After the 20-day intervention, significantly greater clinical improvement was observed in the rTMS group relative to the sham group across multiple symptom domains (Fig. 2). For the PANSS Negative subscale, the rTMS group showed lower scores than in the sham group at the end of treatment (16.09 ± 4.46 vs.18.82 ± 6.15; t = -2.351, p = 0.021, Cohen's d = 0.514). Similarly, PANSS General Psychopathology scores were reduced in the rTMS group compared with the sham group (29.71 ± 4.73 vs. 34.03 ± 6.19; t = -3.615, p < 0.001, Cohen's d = 0.791). Consistently, the total score of PANSS was lower following rTMS than following sham stimulation (58.18 ± 10.21 vs. 66.77 ± 14.90; t = -3.117, p = 0.003, Cohen's d = 0.682). No significant difference between-group was detected for PANSS Positive symptoms.

Functional recovery was also greater in the rTMS group, as indicated by higher GAF scores relative to the sham group (51.64 ± 8.15 vs. 46.56 ± 11.73; t = 2.330, p = 0.022, Cohen's d = 0.510). In addition, lower post-treatment CGI scores were observed in the rTMS group compared to the sham group (8.44 ± 0.92 vs. 8.97 ± 1.18; t = -2.311, p = 0.023, Cohen's d = 0.506), indicating reduced illness severity.

3.3. Alterations in functional gradient topography

The principal functional gradient (G1) was computed to characterize the macroscale cortical hierarchy spanning from unimodal sensorimotor system to transmodal cognitive networks. As depicted in Fig. 3a, a continuous and reproducible gradient organization was observed across all subgroups. The first gradient component explained the largest proportion of connectome variance (25.84%, Fig. 3b), supporting its role as the dominant axis of cortical organization. Global shifts in the gradient distribution were assessed using the Kolmogorov-Smirnov (KS) test. A significant longitudinal alteration in the distribution of G1 scores was observed within the rTMS group following treatment (D = 0.289, p = 0.046), with a moderate effect size (Cohen's d = -0.319). No significant distributional changes were detected in the sham group (p > 0.05) (Fig. 3c).

To localize treatment-related effects, post-treatment G1 scores were compared between the rTMS and sham groups at the nodal level (Fig. 3d). Multiple comparisons across nodes were controlled using FDR correction, and significant between-group differences were identified in three regions that survived this correction. Specifically, elevated gradient scores were found in the rTMS group relative to the sham group in the right middle occipital gyrus (MOG; t = 3.971, p < 0.001) and the right angular gyrus (ANG; t = 3.303, p < 0.001). Conversely, reduced gradient scores were observed in the right anterior cingulate cortex (ACC; t = -3.059, p = 0.002).

System-level effects were further evaluated by aggregating gradient scores within the seven canonical networks (Fig. 3e). A significant group difference was observed in the ventral attention network (VAN) at the post-treatment, with reduced G1 scores in the rTMS group compared with the sham group (t = -2.00, p = 0.045). Moreover, the network-wise distribution of t-statistics across networks indicated that positive shifts (rTMS > Sham) were predominantly concentrated in the somatomotor network (SMN) and default mode network (DMN), whereas negative shifts were primarily localized to the VAN (Fig. 3f).

Table 1
Demographic and clinical variables in patients with first-episode schizophrenia in active and sham rTMS groups.

	rTMS (n = 45)	Sham (n = 39)	t /χ^2	p
Age	27.05 ± 8.23	26.34 ± 7.99	0.400	0.690
Sex(female)	23(22)	16(22)	0.671	0.413
Education (year)	11.67 ± 4.01	10.79 ± 3.68	1.032	0.305
DUP (month)	13.25 ± 22.23	17.45 ± 18.67	0.930	0.355

Note: DUP, duration of untreated psychosis.

3.4. Functional characterization and cognitive decoding of gradient alterations

The spatial distribution of t-statistics reflecting post-treatment group differences (rTMS vs. Sham) was mapped onto the cortical surface (Fig. 4a). A hierarchical divergence was observed in the resulting maps. Positive t-values were predominantly localized to transmodal association areas, including regions within the default mode and frontoparietal networks, whereas negative t-values were primarily concentrated in unimodal sensorimotor and attentional territories. Despite these regionally specific shifts, global properties of the principal gradient were preserved. As shown in Fig. 4b, no significant between-group differences were observed in post-treatment global gradient metrics, including gradient range, gradient variance, and explained ratio (all p > 0.05).

To interpret the functional relevance of these regional patterns, quantitative meta-analytic decoding was performed using the Neurosynth database. The spatial pattern of positive t-values was associated with higher-order cognitive domains. As illustrated in Fig. 4c, enriched terms included executive and mnemonic processes, such as working memory, executive control, memory retrieval, reasoning, and recognition. In contrast, the spatial pattern of negative t-values was predominantly linked to primary sensory and perceptual functions. As shown in Fig. 4d, strong associations were observed with terms including auditory perception, visual motion, speech sounds, listening, and multisensory processing.

3.5. Transcriptomic signatures underlying gradient reorganization

Genes exhibiting significant positive PLS weights (PLS+, Z > 5), were enriched for biological processes related to neural development and structural organization, including spinal cord development, glial cell development, regulation of cell division, and actin filament bundle assembly (Fig. 5a). CSEA revealed that these PLS + gene set were significantly enriched in cortical interneurons, oligodendrocytes, and cerebellar astrocytes (FDR-corrected p < 0.05; Fig. 5b). Developmental and regional profiling additionally indicated preferential expression in the amygdala and cerebellum during early adulthood (Fig. 5c).

Conversely, genes with significant negative PLS weights (PLS-, Z < 5), were primarily enriched for transmembrane transport and metabolic regulation, including metal ion transport, potassium/inorganic cation transmembrane transport, and glycosphingolipid biosynthetic processes (Fig. 5d). In CSEA, the PLS- gene set was significantly enriched in brainstem cholinergic neurons and spinal cord motor neurons (FDR-corrected p < 0.05; Fig. 5e). Regionally, elevated expressed was observed in the cerebellum and thalamus across adult developmental stages (Fig. 5f).

3.6. Prediction of treatment response based on baseline gradient topography

To determine whether baseline functional hierarchy serves as a

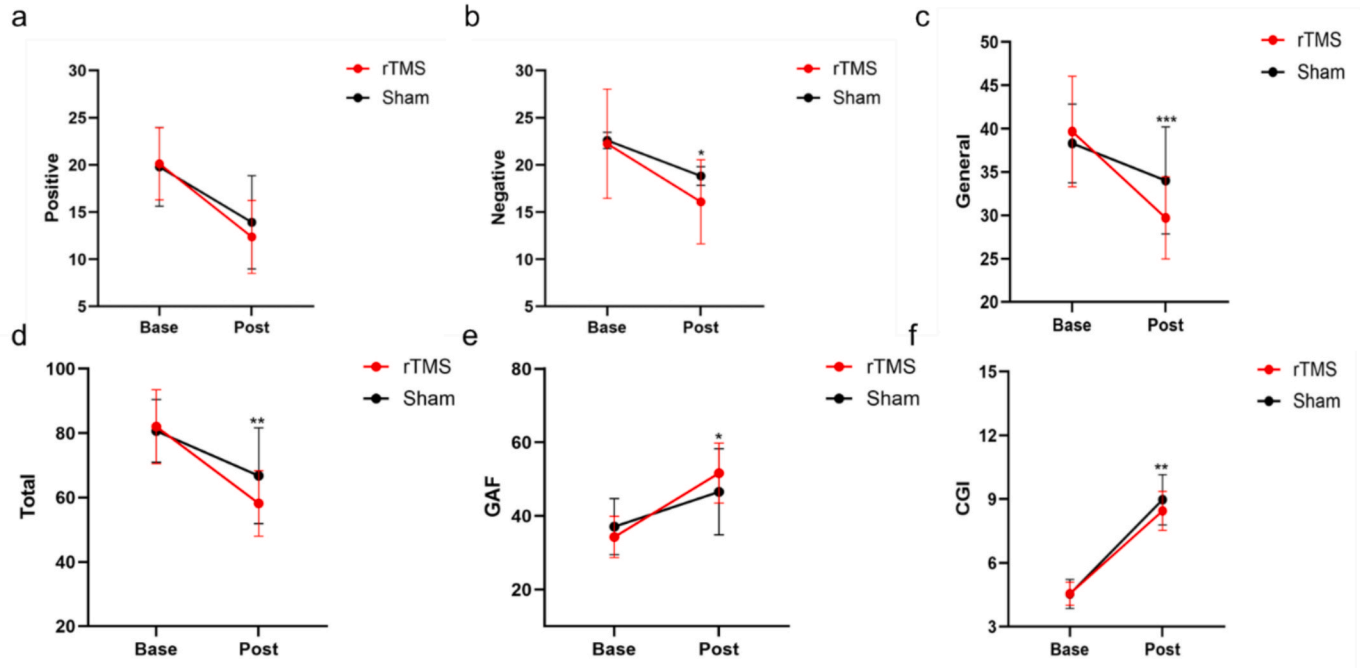

Fig. 2. Comparison of clinical outcomes between active and sham rTMS groups. Trajectories of clinical scores from baseline to post-treatment (4 weeks) are shown for (A) PANSS Positive subscale, (B) PANSS Negative subscale, (C) PANSS General Psychopathology subscale, (D) PANSS Total score, (E) Global Assessment of Functioning (GAF), and (F) Clinical Global Impression (CGI). * $p < 0.05$, ** $p < 0.01$, *** $p < 0.001$. PANSS, Positive and Negative Syndrome Scale.

biomarker for therapeutic efficacy, a unified PLS regression framework was implemented to test moderating effect of baseline gradient features on clinical improvement. At the nodal level, baseline gradient variation in specific regions showed modest associations with improvement in negative symptom in the rTMS group. The strongest nodal effect was observed for node 226 ($R^2 = 0.015$, $p = 0.033$), corresponding anatomically to the right MOG. As illustrated in Fig. 6a, this interaction suggested that baseline gradient topography in this region was differentially associated with symptom change across treatment group. Although the explained variance was small, the contribution of this regions was supported by the PLS weight rankings (weigh = 0.095; Fig. 6b) and VIP profile (VIP = 2.691; Fig. 6c).

At the subnetwork level, the VAN emerged as a more robust moderator of improvement in general psychopathology ($R^2 = 0.163$, p = 0.009). A significant interaction between baseline VAN gradient scores and symptom change was observed (Fig. 6d). Consistently, the VAN showed the highest positive PLS weight among all the canonical networks (weight = 0.539; Fig. 6e) and was the only network exceeding the VIP threshold of 1.0 for prediction of general psychopathology improvement (VIP = 1.835; Fig. 6f). These findings suggest that baseline gradient organization may carry modest but potentially meaningful information related to treatment responsiveness, although independent validation will be required before stronger biomarker claims can be made.

4. Discussion

To the best of our knowledge, the present study provides the first multiscale account of the therapeutic mechanisms of low-frequency (1-Hz) rTMS applied to the right OFC in drug-naïve, first-episode schizophrenia. By integrating a randomized controlled trial framework with macroscale connectome gradient mapping and microscale imaging transcriptomics, several convergent findings were obtained. First, active stimulation was accompanied by a reconfiguration of the cortical functional hierarchy, reflected by a longitudinal shift in the distribution of the principal functional gradient and regionally specific changes spanning transmodal and attentional systems. Second, these spatially resolved gradient alterations were statistically coupled to cortical gene expression patterns enriched for neurodevelopmental and glial-related processes, with cell-type signatures implicating interneuronal and oligodendroglia components. Finally, baseline gradient topography within visual and ventral attention systems moderated clinical response, supporting the potential utility of functional hierarchy metrics as candidate biomarkers for treatment stratification in precision psychiatry. These findings suggest that inhibitory OFC-rTMS may confer clinical benefit by reshaping large-scale cortical hierarchy and by engaging molecular programs related to circuit stabilization and plasticity, potentially contributing to restoration of excitation-inhibition balance and network communication efficiency.

4.1. The orbitofrontal cortex as a target for negative symptom modulation

The observed reduction in negative symptoms following right OFC stimulation reinforces the putative involvement of OFC-centered circuitry in the pathophysiology of schizophrenia. The OFC occupies a strategic position within fronto-striatal-thalamic loops that support reward valuation, emotion regulation, and goal-directed decision-making, domains that are frequently compromised in schizophrenia patients with negative symptoms (Rolls, 2019; Shukla et al., 2019b). Structural and functional abnormalities of the OFC have been repeatedly reported in first-episode schizophrenia, with links to anhedonia and avolition (Walton et al., 2018). These results add to emerging evidence that the OFC-targeted neuromodulation may represent a viable alternative when conventional targets (e.g., DLPFC) yield limited effects, particularly for negative-symptom domains (Barr et al., 2012; Wobrock et al., 2015). Mechanistically, 1-Hz rTMS is generally considered to reduce cortical excitability and can modulate distributed networks via transsynaptic effects (Fitzgerald et al., 2006). In this context, a plausible interpretation is that inhibitory OFC stimulation attenuates maladaptive hyperactivity/hyperconnectivity within OFC-limbic-striatal circuitry, thereby reducing neural noise and improving top-down modulation of reward and salience processing (Downar, 2019).This account is consistent with neurophysiological evidence from the present cohort indicating modulation of cortical plasticity and oscillatory dynamics following OFC-

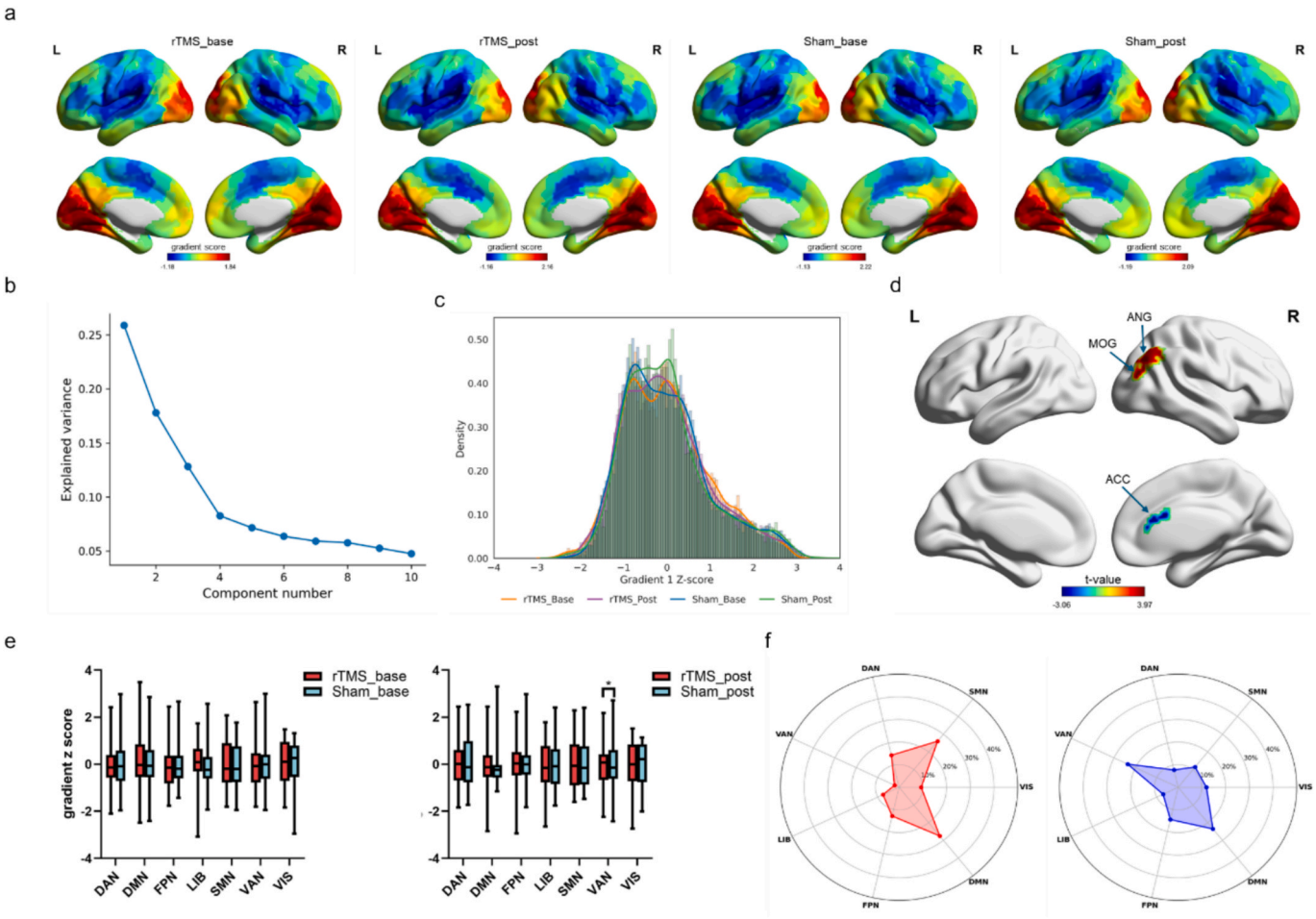

Fig. 3. Alterations in the principal functional gradient following rTMS treatment. (a) Surface visualization of the principal functional gradient (G1) across groups, spanning from unimodal (cool colors) to transmodal (warm colors) regions. (b) Scree plot showing G1 explains 25.84% of connectome variance. (c) Density plots of G1 scores; a significant longitudinal shift was observed in the active group (KS test, $D = 0.289$, $p = 0.046$). (d) Regions showing significant post-treatment group differences. Warm colors denote higher scores in the active group (e.g., MOG, ANG), while cool colors denote lower scores (e.g., ACC). (e) Boxplots of averaged G1 scores within canonical several networks; the Ventral Attention Network (VAN) differed significantly post-treatment ($t = 2.00$, $p < 0.05$). (f) Radar charts showing the distribution of t-statistics across subnetworks. Abbreviations: ACC, Anterior Cingulate Cortex; ANG, Angular Gyrus; DAN, Dorsal Attention Network; DMN, Default Mode Network; FPN, Frontoparietal Network; LIM, Limbic Network; MOG, Middle Occipital Gyrus; SMN, Somatomotor Network; VAN, Ventral Attention Network; VIS, Visual Network.

rTMS (Jiao et al., 2024).

4.2. *Reshaping the macroscale functional hierarchy*

A core finding was the rTMS- associated reorganization of the principal functional gradient, which captures the dominant axis of cortical hierarchy extending from unimodal sensory systems to transmodal association cortex (Ito and Murray, 2023). Schizophrenia has been widely conceptualized as a disorder of dysconnection (Friston, 1998) in which hierarchical integration is compressed (Dong et al., 2025; Holmes et al., 2023), thereby impairing the coordination of sensory evidence with higher-order cognition and predictive control. Within this framework, the significant post-treatment shift in the global gradient distribution of G1 scores observed in the rTMS group reflects a system-level renormalization of intrinsic functional organization (Raut et al., 2020).

At the regional level, treatment effects were spatially differentiated. Increased gradient scores in the right MOG and ANG, indicating a shift towards the transmodal end of the hierarchy. Such elevation may reflect an enhanced functional differentiation from lower-level sensory constraints and improved integration with association systems supporting memory, executive processing, and multimodal inference (Mesulam, 1998). In parallel, decreased gradient scores were found in the right ACC, suggesting a relative downshifting of attentional control components. Suppression of ACC hierarchy may contribute to improvement in general psychopathology (Menon, 2011). These bidirectional changes are consistent with a coordinated rebalancing between transmodal association cortex and salience/attentional systems, potentially supporting improved allocation of cognitive resources and reduced maladaptive salience signaling following inhibitory OFC stimulation.

4.3. *Transcriptomic underpinnings of gradient reorganization*

By linking macroscale gradient effects to transcriptomic variation, putative molecular substrates driving the observed network reconfiguration were delineated. The distinct spatial patterns of gene expression associated with gradient increases and decreases suggest that divergent biological pathways are recruited to restore the cortical hierarchy. Regions exhibiting gradient increases were associated with genes enriched for neural development, cytoskeletal organization, and glial cell differentiation. These biological processes constitute the foundational machinery of synaptic plasticity and structural remodeling(Gordon-Weeks and Fournier, 2014; Langle et al., 2002; Wang et al., 2016). Consequently, 1-Hz OFC-rTMS may facilitate the remodeling of transmodal networks by modulating synaptic efficacy and structural connectivity,

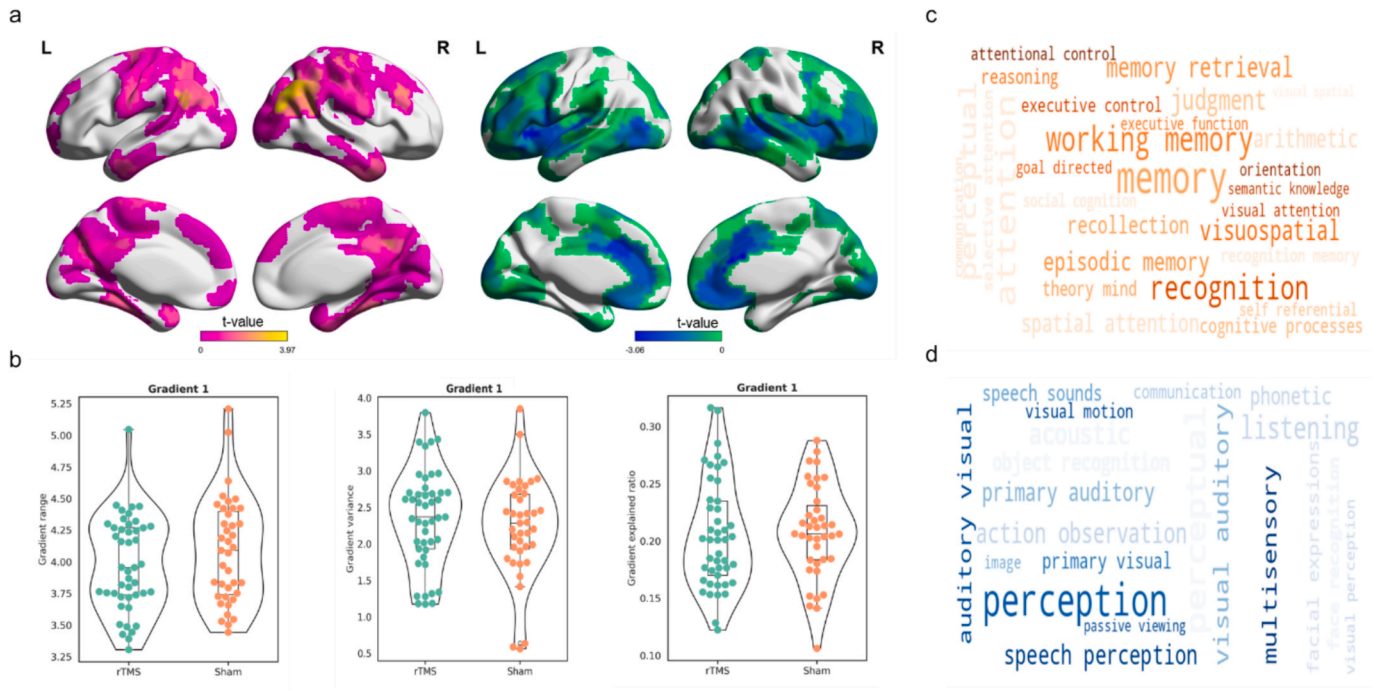

Fig. 4. Functional characterization and cognitive decoding of gradient alterations. (a) Cortical surface maps displaying the spatial distribution of t-statistics for the post-treatment comparison between active and sham groups. Warm colors indicate regions with positive t-values (Active > Sham), while cool colors indicate negative t-values (Active < Sham).(b) Violin plots comparing global gradient metrics (gradient range, variance, and explained ratio) between groups at post-treatment. No significant differences were observed ($p > 0.05). (c) Word cloud visualizing the cognitive terms associated with the spatial map of positive t-values, highlighting enrichment in higher-order functions such as working memory and executive control. (d) Word cloud visualizing the cognitive terms associated with the spatial map of negative t-values, highlighting enrichment in sensory and perceptual domains such as auditory and visual perception. The size of the text corresponds to the strength of the correlation with the *meta*-analytic maps.

thereby countering the synaptic paucity characteristic of schizophrenia (Garey et al., 1998).

Cell-type enrichment analyses further revealed that these gradient-enhancing effects are likely mediated by specific cellular populations, primarily cortical interneurons oligodendrocytes, and cerebellar astrocytes. The specific implication of interneurons aligns with the GABAergic deficit hypothesis of schizophrenia, which posits that dysfunction of parvalbumin-positive interneurons disrupts gamma oscillations and cognitive integration (Lewis et al., 2012). These findings imply that the normalization of inhibitory circuitry may be promoted by rTMS, potentially restoring the excitation/inhibition balance necessary for precise signal processing (Lisman et al., 2008). Additionally, the strong signal for oligodendrocytes resonates with extensive evidence of white matter dysconnectivity and myelination deficits in the disorder (Davis et al., 2003). This suggests that the therapeutic plasticity induced by rTMS extends beyond neuronal synapses to encompass adaptive myelination, a process essential for optimizing the conduction velocity and the long-range coupling of high-order networks (Monje, 2018). Furthermore, the enrichment of cerebellar astrocytes, coupled with preferential expression profiles in the amygdala and cerebellum during early adulthood, points to a potential modulation of cortico-cerebellar-limbic loops. Such network-level modulation may facilitate the stabilization of emotional regulation and motor-cognitive integration, processes often disrupted in early-stage psychosis (Andreasen et al., 1998; Faris et al., 2024).

Conversely, regions exhibiting gradient decreases were linked to genes enriched for ion transport and metabolic regulation. The enrichment of ion channel genes suggests that the suppressive effects of 1-Hz rTMS are mechanistically anchored in the modulation of membrane excitability. By influencing the expression or function of voltage-gated ion channels, aberrant hyperactivity often observed in the salience network of patients with psychosis may be downregulated (Supekar et al., 2019). This calming effect on neural firing rates would directly contribute to the observed reduction in gradient scores, reflecting a functional segregation of these regions from excessive sensory integration. Furthermore, the association with metabolic pathways points to the high energetic cost of maintaining the functional hierarchy of brain. Given that hyperactive regions in schizophrenia place a heavy metabolic burden on the brain (Rossetti et al., 2024), metabolic homeostasis may be restored by the rTMS-induced suppression of these regions. This process reduces the oxidative stress and energetic demands associated with neural noise, thereby allowing resources to be reallocated to more efficient cognitive processing (Richiardi et al., 2015). Finally, cell-type enrichment analysis provided further context, revealing significant enrichment in brainstem cholinergic neurons and spinal cord motor neurons, with elevated expression observed in the cerebellum and thalamus. The implication of these subcortical and brainstem populations suggests that the top-down inhibition exerted by OFC stimulation may not be confined to the cortex but may propagate to arousal and motor regulatory centers (Higley and Picciotto, 2014). This descending modulation could potentially dampen the hyper-arousal states and psychomotor agitation often associated with psychotic symptomatology (Walther and Strik, 2012).

4.4. *Functional gradients as predictive biomarkers*

Using a unified PLS framework, distinct baseline hierarchical features were identified as predictors for different clinical outcomes, suggesting a double dissociation in the predictive mechanisms of symptom domains. At the nodal level, the baseline gradient score in the right MOG predicted improvement in negative symptoms following active rTMS. Although classically considered a categorized as a primary visual region, the MOG is functionally integral to the early stages of social perception, particularly in the decoding of facial emotions and biological motion (Green et al., 2008). In schizophrenia, deficits in these lower-level visual inputs serve as a bottleneck, constraining the performance of

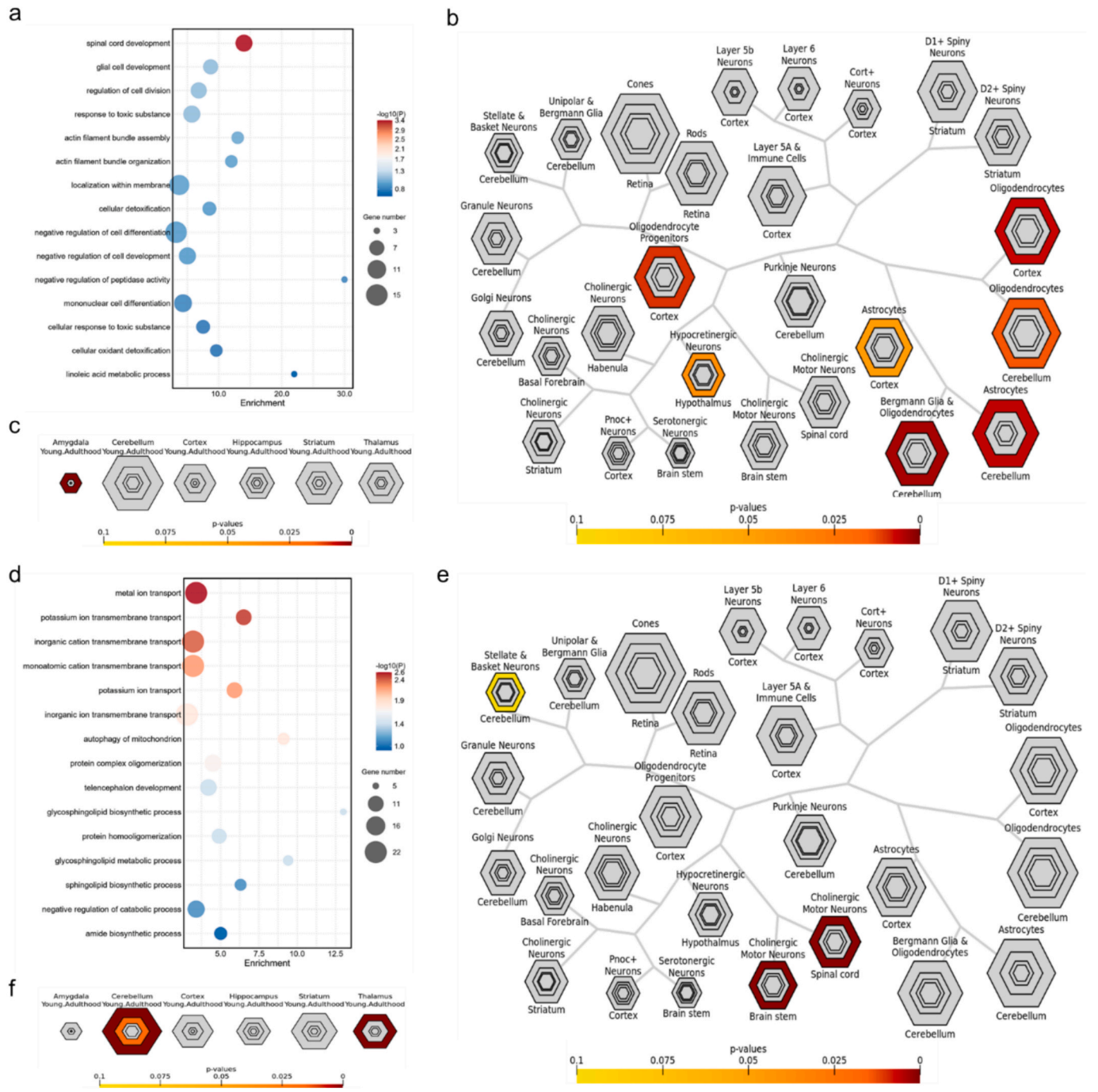

Fig. 5. Transcriptomic enrichment and cell-type specificity of gradient-associated genes. (a) Gene Ontology (GO) enrichment analysis for genes with positive PLS weights (PLS +). (b) Cell-type specific expression analysis (CSEA) for PLS + genes. (c) CSEA results for adult human brain regions, showing enrichment of PLS + genes in the amygdala and cerebellum. (d) GO enrichment analysis for genes with negative PLS weights (PLS-). (e) CSEA results for PLS- genes. (f) CSEA results for adult human brain regions.

downstream socio-cognitive and motivational networks (Herrmann et al., 2006). Consequently, the baseline hierarchical positioning of the MOG may index the functional integrity or plasticity reserve of the visual-social interface, determining the capacity of brain to translate OFC modulation into improved social engagement and affective responsiveness.

At the network level, the baseline hierarchy of the VAN predicted improvement in general psychopathology. This finding aligns with the aberrant salience hypothesis of psychosis, which posits that a dysregulated salience system misattributes significance to neutral internal or external stimuli, thereby fueling anxiety, tension, and disorganized behavior, core components of the general psychopathology subscale (Kapur, 2003; Palaniyappan and Liddle, 2012). The VAN acts as a circuit breaker that reorients attention to behaviorally relevant events. In early-stage schizophrenia, this network is often hyperactive or inappropriately integrated with other systems, leading to a state of hyperarousal (Uddin, 2015). Since 1-Hz rTMS exerts an inhibitory effect (Lefaucheur et al., 2020), patients with specific baseline VAN gradient configurations, likely reflecting a state of pathological hyper-integration (Puledda et al., 2021), may be optimally primed to benefit from the suppressive, noise-canceling effects of OFC stimulation. By attenuating aberrant signaling within salience-related circuitry, rTMS may restore the threshold for

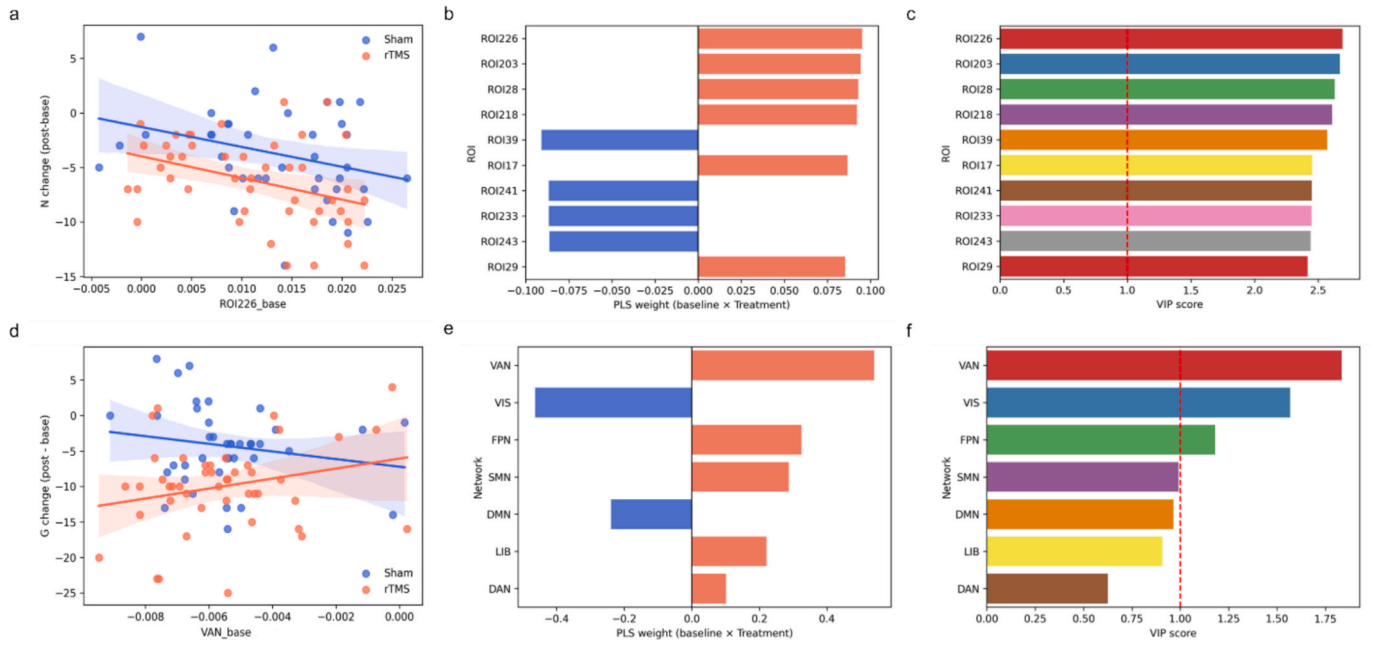

Fig. 6. Prediction of clinical improvement based on baseline functional gradient features. (a) Scatter plot illustrating the interaction between baseline gradient scores of ROI 226 (right Middle Occipital Gyrus) and the change in negative symptoms (post-base). Regression lines are separated by group (Red: rTMS; Blue: Sham). (b) Bar chart displaying the PLS interaction weights for the top 10 predictive ROIs associated with negative symptom improvement. (c) Bar chart showing the Variable Importance in Projection (VIP) scores for the top 10 ROIs; the red dashed line indicates the significance threshold (VIP > 1.0). (d) Scatter plot illustrating the interaction between baseline gradient scores of the Ventral Attention Network (VAN) and the change in general psychopathology symptoms. (e) Bar chart displaying the PLS interaction weights for the seven canonical subnetworks associated with general symptom improvement. (f) Bar chart showing the VIP scores for the subnetworks; the VAN is the only network exceeding the threshold of 1.0. (For interpretation of the references to colour in this figure legend, the reader is referred to the web version of this article.)

salience detection and reduce maladaptive attentional capture, thereby directly alleviating distress and agitation indexed by general psychopathology measures (Han et al., 2020; Wang et al., 2017).

Several limitations warrant consideration. First, while the present sample is substantial for a drug-naïve, first-episode cohort, independent replication across sites will be essential to establish the robustness and generalizability of both the gradient effects and the predictive markers. Second, the associations among stimulation, gradient reorganization, and clinical improvement should not be interpreted as evidence of causality, and the molecular and cellular mechanisms inferred from the transcriptomic analyses require direct experimental validation. Third, transcriptomic inference was based on AHBA data derived from a limited number of healthy adult donors. Although this approach is widely used in imaging-transcriptomic studies, it cannot capture disease-specific or individual-level expression profiles relevant to schizophrenia. Fourth, the resting-state fMRI acquisition duration was relatively short (approximately 6 min), which may have limited the reliability of functional connectivity estimation and, consequently, the stability of gradient reconstruction. Fifth, stimulation targeting was based on the AF8 scalp coordinate in the international 10–10 EEG system rather than individualized neuronavigation. Although this approach is practical and commonly used in clinical settings, it may not fully account for inter-individual variability in cranio-cortical anatomy and therefore may have introduced variability in the precise OFC subregion stimulated across participants. Sixth, the coil-flip sham procedure may not have constituted a fully inert placebo condition, given the potential for residual field exposure and incomplete matching of the somatosensory features of active OFC stimulation. Moreover, blinding efficacy was not formally assessed, and E-field simulations were not performed. These issues should be addressed in future studies through longer resting-state acquisitions, formal blinding assessments, MRI-guided neuronavigation, and precise electromagnetic field modeling.

5. Conclusion

In summary, this study investigated the therapeutic efficacy and underlying multiscale mechanisms of low-frequency rTMS targeting the OFC in drug-naïve first-episode schizophrenia. Active stimulation was associated with clinical improvement in negative symptoms and with a system-level renormalization of macroscale cortical hierarchy. Gradient reorganization was characterized by enhanced segregation of transmodal networks and attenuation of aberrant salience-related processing and was spatially linked to transcriptomic signatures implicating inhibitory and glial-related mechanisms. Baseline gradient topography further predicted symptom change, indicating that treatment susceptibility was conditioned by pre-existing functional architecture. These findings support the OFC as a viable neuromodulation target in early-stage psychosis and highlight functional gradient metrics as candidate biomarkers to inform individualized rTMS strategies.

CRediT authorship contribution statement

Wenwen Miao: Writing – review & editing, Writing – original draft, Visualization, Validation, Methodology, Investigation, Formal analysis, Data curation. **Xiong Jiao:** Writing – review & editing, Writing – original draft, Visualization, Validation, Methodology, Investigation, Formal analysis, Data curation, Conceptualization. **Ningning Zeng:** Writing – review & editing, Writing – original draft, Visualization, Validation, Methodology, Investigation, Formal analysis, Data curation. **Min Wang:** Writing – review & editing, Writing – original draft, Visualization, Validation, Methodology, Investigation, Formal analysis, Data curation. **Kexu Zhang:** Writing – review & editing, Writing – original draft, Visualization, Validation, Methodology, Investigation, Formal analysis, Data curation. **Cheng Yang:** Writing – review & editing, Writing – original draft, Visualization, Validation, Methodology, Investigation, Formal analysis, Data curation. **Yuanjun Xie:** Writing – review &

editing, Writing – original draft, Visualization, Validation, Methodology, Investigation, Formal analysis, Data curation. **Ziliang Wang:** Writing – review & editing, Writing – original draft, Visualization, Validation, Methodology, Investigation, Funding acquisition, Formal analysis, Data curation. **Qiang Hu:** Writing – review & editing, Writing – original draft, Visualization, Validation, Project administration, Methodology, Investigation, Funding acquisition, Formal analysis, Data curation, Conceptualization.

Funding

This work was supported by Jianghuai Talent Training Program team project (No. 2025jh18), Annual Artificial Intelligence Scenario Innovation Project of Anhui Province (No. 2026cx), Wuhu Science and Technology Program (No. 2025kj011), Clinical Medical Research Conversion Special for Anhui Key Research and Development Program (No. 202204295107020065), Jiangsu Natural Science Foundation Youth Project (No. BK20240506), Research Foundation of Jiangsu Provincial Commission of Health and Family planning (No. H2023036, No. H2024099), and Jiangsu Provincial Administration of Traditional Chinese Medicine Project (No. MS2024122).

Declaration of Competing Interest

The authors declare that they have no known competing financial interests or personal relationships that could have appeared to influence the work reported in this paper.

Acknowledgement

We would like to thank the participants who contributed their time to completing these research studies.

Data availability

Data will be made available on request.

References

Andreasen, N.C., Paradiso, S., O'Leary, D.S., 1998. "Cognitive dysmetria" as an integrative theory of schizophrenia: a dysfunction in cortical-subcortical-cerebellar circuitry? Schizophr. Bull. 24 (2), 203–218.
Barr, M.S., Farzan, F., Tran, L.C., Fitzgerald, P.B., Daskalakis, Z.J., 2012. A randomized controlled trial of sequentially bilateral prefrontal cortex repetitive transcranial magnetic stimulation in the treatment of negative symptoms in schizophrenia. Brain Stimul. 5 (3), 337–346.
Blyth, S.H., Cruz Bosch, C., Raffoul, J.J., Chesley, J., Johnson, B., Borodge, D., Sagarwala, R., Masters, R., Brady Jr., R.O., Vandekar, S., Ward, H.B., 2025. Safety of rTMS for schizophrenia: a systematic review and meta-analysis. Schizophr. Bull. 51 (2), 392–400.
Ciric, R., Wolf, D.H., Power, J.D., Roalf, D.R., Baum, G.L., Ruparel, K., Shinohara, R.T., Elliott, M.A., Eickhoff, S.B., Davatzikos, C., Gur, R.C., Gur, R.E., Bassett, D.S., Satterthwaite, T.D., 2017. Benchmarking of participant-level confound regression strategies for the control of motion artifact in studies of functional connectivity. Neuroimage 154 (7), 174–187.
Datta, S., 2018. Exploring relationships in gene expressions: a partial least squares approach. Gene Expr. 9 (6), 249–255.
Davis, K.L., Stewart, D.G., Friedman, J.I., Buchsbaum, M., Harvey, P.D., Hof, P.R., Buxbaum, J., Haroutunian, V., 2003. White matter changes in schizophrenia: evidence for myelin-related dysfunction. Arch. Gen. Psychiatry 60 (5), 443–456.
Dong, D., Wang, Y., Zhou, F., Chang, X., Qiu, J., Feng, T., He, Q., Lei, X., Chen, H., 2025. Functional connectome hierarchy in schizotypy and its associations with expression of schizophrenia-related genes. Schizophr. Bull. 51 (1), 145–158.
Dong, D., Yao, D., Wang, Y., Hong, S.-J., Genon, S., Xin, F., Jung, K., He, H., Chang, X., Duan, M., Bernhardt, B.C., Margulies, D.S., Sepulcre, J., Eickhoff, S.B., Luo, C., 2023. Compressed sensorimotor-to-transmodal hierarchical organization in schizophrenia. Psychol. Med. 53 (3), 771–784.
Dougherty, J.D., Schmidt, E.F., Nakajima, M., Heintz, N., 2010. Analytical approaches to RNA profiling data for the identification of genes enriched in specific cells. Nucleic Acids Res. 38 (13), 4218–4230.
Downar, J., 2019. Orbitofrontal cortex: a 'non-rewarding' new treatment target in depression? Curr. Biol. 29 (5), 896.
Endicott, J., Spitzer, R.L., Fleiss, J.L., Cohen, J., 1976. The global assessment scale: a procedure for measuring overall severity of psychiatric disturbance. Arch. Gen. Psychiatry 33 (6), 766–771.
Faris, P., Pischedda, D., Palesi, F., D'Angelo, E., 2024. New clues for the role of cerebellum in schizophrenia and the associated cognitive impairment. Frontier in Cellular Neuroscience 18 (5), 1386583.
Farrés, M., Platikanov, S., Tsakovski, S., Tauler, R., 2015. Comparison of the variable importance in projection (VIP) and of the selectivity ratio (SR) methods for variable selection and interpretation. J. Chemom. 29 (10), 528–536.
Fitzgerald, P.B., Fountain, S., Daskalakis, Z.J., 2006. A comprehensive review of the effects of rTMS on motor cortical excitability and inhibition. Clin. Neurophysiol. 117 (12), 2584–2596.
Forkmann, T., Scherer, A., Boecker, M., Pawelzik, M., Jostes, R., Gauggel, S., 2011. The clinical global impression scale and the influence of patient or staff perspective on outcome. BMC Psychiatry 11 (1), 83.
Freitas, C., Fregni, F., Pascual-Leone, A., 2009. Meta-analysis of the effects of repetitive transcranial magnetic stimulation (rTMS) on negative and positive symptoms in schizophrenia. Schizophr. Res. 108 (1), 11–24.
Friston, K.J., 1998. The disconnection hypothesis. Schizophr. Res. 30 (2), 115–125.
Friston, K.J., 1999. Schizophrenia and the disconnection hypothesis. Acta Psychiatr. Scand. 99 (s395), 68–79.
Garey, L.J., Ong, W.Y., Patel, T.S., Kanani, M., Davis, A., Mortimer, A.M., Barnes, T.R.E., Hirsch, S.R., 1998. Reduced dendritic spine density on cerebral cortical pyramidal neurons in schizophrenia. J. Neurol. Neurosurg. Psychiatry 65 (4), 446–453.
Gordon-Weeks, P.R., Fournier, A.E., 2014. Neuronal cytoskeleton in synaptic plasticity and regeneration. J. Neurochem. 129 (2), 206–212.
Green, M.F., Penn, D.L., Bentall, R., Carpenter, W.T., Gaebel, W., Gur, R.C., Kring, A.M., Park, S., Silverstein, S.M., Heinssen, R., 2008. Social cognition in schizophrenia: an NIMH workshop on definitions, assessment, and research opportunities. Schizophr. Bull. 34 (6), 1211–1220.
Han, S., Becker, B., Duan, X., Cui, Q., Xin, F., Zong, X., Hu, M., Yang, M., Li, R., Yu, Y., Liao, W., Chen, X., Chen, H., 2020. Distinct striatum pathways connected to salience network predict symptoms improvement and resilient functioning in schizophrenia following risperidone monotherapy. Schizophr. Res. 215 (1), 89–96.
He, H., Lu, J., Yang, L., Zheng, J., Gao, F., Zhai, Y., Feng, J., Fan, Y., Ma, X., 2017. Repetitive transcranial magnetic stimulation for treating the symptoms of schizophrenia: a PRISMA compliant meta-analysis. Clin. Neurophysiol. 128 (5), 716–724.
Herrmann, M.J., Reif, A., Jabs, B.E., Jacob, C., Fallgatter, A.J., 2006. Facial affect decoding in schizophrenic disorders: a study using event-related potentials. Psychiatry Res. 141 (3), 247–252.
Higley, M.J., Picciotto, M.R., 2014. Neuromodulation by acetylcholine: examples from schizophrenia and depression. Curr. Opin. Neurobiol. 29 (12), 88–95.
Holmes, A., Levi, P.T., Chen, Y.-C., Chopra, S., Aquino, K.M., Pang, J.C., Fornito, A., 2023. Disruptions of hierarchical cortical organization in early psychosis and schizophrenia. Biol. Psychiatry: Cognit. Neurosci. Neuroimaging 8 (12), 1240–1250.
Hong, S.-J., Xu, T., Nikolaidis, A., Smallwood, J., Margulies, D.S., Bernhardt, B., Vogelstein, J., Milham, M.P., 2020. Toward a connectivity gradient-based framework for reproducible biomarker discovery. Neuroimage 223 (12), 117322.
Hu, Q., Jiao, X., Zhou, J., Tang, Y., Zhang, T., Song, C., Wang, J., Xiao, Q., Ye, J., Sun, J., Wang, X., Li, C., Wang, J., 2023. Low-frequency repetitive transcranial magnetic stimulation over the right orbitofrontal cortex for patients with first-episode schizophrenia: a randomized, double-blind, sham-controlled trial. Psychiatry Res. 330 (11), 115600.
Huntenburg, J.M., Bazin, P.-L., Margulies, D.S., 2018. Large-scale gradients in human cortical organization. Trends Cogn. Sci. 22 (1), 21–31.
Ito, T., Murray, J.D., 2023. Multitask representations in the human cortex transform along a sensory-to-motor hierarchy. Nat. Neurosci. 26 (2), 306–315.
Jiao, X., Hu, Q., Tang, Y., Zhang, T., Zhang, J., Wang, X., Sun, J., Wang, J., 2024. Abnormal global cortical responses in drug-naïve patients with schizophrenia following orbitofrontal cortex stimulation: a concurrent transcranial magnetic stimulation–electroencephalography study. Biol. Psychiatry 96 (5), 342–351.
Kapur, S., 2003. Psychosis as a state of aberrant salience: a framework linking biology, phenomenology, and pharmacology in schizophrenia. Am. J. Psychiatry 160 (1), 13–23.
Kay, S.R., Fiszbein, A., Opler, L.A., 1987. The positive and negative syndrome scale (PANSS) for schizophrenia. Schizophr. Bull. 13 (2), 261–276.
Krishnan, A., Williams, L.J., McIntosh, A.R., Abdi, H., 2011. Partial least squares (PLS) methods for neuroimaging: a tutorial and review. Neuroimage 56 (2), 455–475.
Langle, S.L., Poulain, D.A., Theodosis, D.T., 2002. Neuronal–glial remodeling: a structural basis for neuronal–glial interactions in the adult hypothalamus. Journal of Physiology-Paris 96 (3), 169–175.
Lefaucheur, J.-P., Aleman, A., Baeken, C., Benninger, D.H., Brunelin, J., Di Lazzaro, V., Filipović, S.R., Grefkes, C., Hasan, A., Hummel, F.C., Jääskeläinen, S.K., Langguth, B., Leocani, L., Londero, A., Nardone, R., Nguyen, J.-P., Nyffeler, T., Oliveira-Maia, A.J., Oliviero, A., Padberg, F., Palm, U., Paulus, W., Poulet, E., Quartarone, A., Rachid, F., Rektorová, I., Rossi, S., Sahlsten, H., Schecklmann, M., Szekely, D., Ziemann, U., 2020. Evidence-based guidelines on the therapeutic use of repetitive transcranial magnetic stimulation (rTMS): an update (2014–2018). Clin. Neurophysiol. 131 (2), 474–528.
Lewis, D.A., Curley, A.A., Glausier, J.R., Volk, D.W., 2012. Cortical parvalbumin interneurons and cognitive dysfunction in schizophrenia. Trends Neurosci. 35 (1), 57–67.
Lisman, J.E., Coyle, J.T., Green, R.W., Javitt, D.C., Benes, F.M., Heckers, S., Grace, A.A., 2008. Circuit-based framework for understanding neurotransmitter and risk gene interactions in schizophrenia. Trends Neurosci. 31 (5), 234–242.

Margulies, D.S., Ghosh, S.S., Goulas, A., Falkiewicz, M., Huntenburg, J.M., Langs, G., Bezgin, G., Eickhoff, S.B., Castellanos, F.X., Petrides, M., Jefferies, E., Smallwood, J., 2016. Situating the default-mode network along a principal gradient of macroscale cortical organization. Proc. Natl. Acad. Sci. 113 (44), 12574–12579.
Markello, R.D., Arnatkeviciute, A., Poline, J.B., Fulcher, B.D., Fornito, A., Misic, B., 2021. Standardizing workflows in imaging transcriptomics with the abagen toolbox. Elife 10 (11), e72129.
Menon, V., 2011. Large-scale brain networks and psychopathology: a unifying triple network model. Trends Cogn. Sci. 15 (10), 483–506.
Mesulam, M.M., 1998. From sensation to cognition. Brain 121 (6), 1013–1052.
Miyamoto, S., Miyake, N., Jarskog, L.F., Fleischhacker, W.W., Lieberman, J.A., 2012. Pharmacological treatment of schizophrenia: a critical review of the pharmacology and clinical effects of current and future therapeutic agents. Mol. Psychiatry 17 (12), 1206–1227.
Monje, M., 2018. Myelin plasticity and nervous system function. Annu. Rev. Neurosci. 41 (41), 61–76.
Murphy, K., Fox, M.D., 2017. Towards a consensus regarding global signal regression for resting state functional connectivity MRI. Neuroimage 154 (7), 169–173.
Ohtani, T., Bouix, S., Hosokawa, T., Saito, Y., Eckbo, R., Ballinger, T., Rausch, A., Melonakos, E., Kubicki, M., 2014. Abnormalities in white matter connections between orbitofrontal cortex and anterior cingulate cortex and their associations with negative symptoms in schizophrenia: a DTI study. Schizophr. Res. 157 (1), 190–197.
Palaniyappan, L., Liddle, P.F., 2012. Does the salience network play a cardinal role in psychosis? an emerging hypothesis of insular dysfunction. J. Psychiatry Neurosci. 37 (1), 17–27.
Power, J.D., Barnes, K.A., Snyder, A.Z., Schlaggar, B.L., Petersen, S.E., 2012. Spurious but systematic correlations in functional connectivity MRI networks arise from subject motion. Neuroimage 59 (3), 2142–2154.
Puledda, F., O'Daly, O., Schankin, C., Ffytche, D., Williams, S.C.R., Goadsby, P.J., 2021. Disrupted connectivity within visual, attentional and salience networks in the visual snow syndrome. Hum. Brain Mapp. 42 (7), 2032–2044.
Raut, R.V., Snyder, A.Z., Raichle, M.E., 2020. Hierarchical dynamics as a macroscopic organizing principle of the human brain. Proc. Natl. Acad. Sci. 117 (34), 20890–20897.
Richiardi, J., Altmann, A., Milazzo, A.-C., Chang, C., Chakravarty, M.M., Banaschewski, T., Barker, G.J., Bokde, A.L.W., Bromberg, U., Büchel, C., Conrod, P., Fauth-Bühler, M., Flor, H., Frouin, V., Gallinat, J., Garavan, H., Gowland, P., Heinz, A., Lemaître, H., Mann, K.F., Martinot, J.-L., Nees, F., Paus, T., Pausova, Z., Rietschel, M., Robbins, T.W., Smolka, M.N., Spanagel, R., Ströhle, A., Schumann, G., Hawrylycz, M., Poline, J.-B., Greicius, M.D., consortium, I., Albrecht, L., Andrew, C., Arroyo, M., Artiges, E., Aydin, S., Bach, C., Banaschewski, T., Barbot, A., Barker, G., Boddaert, N., Bokde, A., Bricaud, Z., Bromberg, U., Bruehl, R., Büchel, C., Cachia, A., Cattrell, A., Conrod, P., Constant, P., Dalley, J., Decideur, B., Desrivieres, S., Fadai, T., Flor, H., Frouin, V., Gallinat, J., Garavan, H., Briand, F.G., Gowland, P., Heinrichs, B., Heinz, A., Heym, N., Hübner, T., Ireland, J., Ittermann, B., Jia, T., Lathrop, M., Lanzerath, D., Lawrence, C., Lemaitre, H., Lüdemann, K., Macare, C., Mallik, C., Mangin, J.-F., Mann, K., Martinot, J.-L., Mennigen, E., Mesquita de Carvahlo, F., Mignon, X., Miranda, R., Müller, K., Nees, F., Nymberg, C., Paillere, M.-L., Paus, T., Pausova, Z., Poline, J.-B., Poustka, L., Rapp, M., Robert, G., Reuter, J., Rietschel, M., Ripke, S., Robbins, T., Rodehacke, S., Rogers, J., Romanowski, A., Ruggeri, B., Schmäl, C., Schmidt, D., Schneider, S., Schumann, M., Schubert, F., Schwartz, Y., Smolka, M., Sommer, W., Spanagel, R., Speiser, C., Spranger, T., Stedman, A., Steiner, S., Stephens, D., Strache, N., Ströhle, A., Struve, M., Subramaniam, N., Topper, L., Whelan, R., Williams, S., Yacubian, J., Zilbovicius, M., Wong, C.P., Lubbe, S., Martinez-Medina, L., Fernandes, A., Tahmasebi, A., 2015. Correlated gene expression supports synchronous activity in brain networks. Science 348(6240), 1241-1244.
Robin, A., Bastin, J., 2025. Role and functions of the human orbitofrontal cortex. J. Clin. Neurophysiol. 42 (7), 609–615.
Rolls, E.T., 2019. The orbitofrontal cortex and emotion in health and disease, including depression. Neuropsychologia 128 (5), 14–43.
Rolls, E.T., 2023. Emotion, motivation, decision-making, the orbitofrontal cortex, anterior cingulate cortex, and the amygdala. Brain Struct. Funct. 228 (5), 1201–1257.
Rolls, E.T., Cheng, W., Feng, J., 2020. The orbitofrontal cortex: reward, emotion and depression. Brain. Communications 2 (2), fcaa196.
Rossetti, M., Stanca, S., Panichi, L.B., Bongioanni, P., 2024. Brain metabolic profiling of schizophrenia: a path towards a better understanding of the neuropathogenesis of psychosis. Metab. Brain Dis. 40 (1), 28.
Rudebeck, P.H., Rich, E.L., 2018. Orbitofrontal cortex. Curr. Biol. 28 (18), R1083–R1088.
Schaefer, A., Kong, R., Gordon, E.M., Laumann, T.O., Zuo, X.-N., Holmes, A.J., Eickhoff, S.B., Yeo, B.T.T., 2018. Local-global parcellation of the human cerebral cortex from intrinsic functional connectivity MRI. Cereb. Cortex 28 (9), 3095–3114.
Shen, E.H., Overly, C.C., Jones, A.R., 2012. The Allen Human Brain Atlas: comprehensive gene expression mapping of the human brain. Trends Neurosci. 35 (12), 711–714.
Shukla, D.K., Chiappelli, J.J., Sampath, H., Kochunov, P., Hare, S.M., Wisner, K., Rowland, L.M., Hong, L.E., 2019a. Aberrant frontostriatal connectivity in negative symptoms of chizophrenia. Schizophr. Bull. 45 (5), 1051–1059.
Shukla, D.K., Chiappelli, J.J., Sampath, H., Kochunov, P., Hare, S.M., Wisner, K., Rowland, L.M., Hong, L.E., 2019b. Aberrant frontostriatal connectivity in negative symptoms of schizophrenia. Schizophr. Bull. 45 (5), 1051–1059.
Siever Larry, J., Davis Kenneth, L., 2004. The pathophysiology of schizophrenia disorders: perspectives from the spectrum. Am. J. Psychiatry 161 (3), 398–413.
Supekar, K., Cai, W., Krishnadas, R., Palaniyappan, L., Menon, V., 2019. Dysregulated brain dynamics in a triple-network saliency model of schizophrenia and its relation to psychosis. Biol. Psychiatry 85 (1), 60–69.
Thomas Yeo, B.T., Krienen, F.M., Sepulcre, J., Sabuncu, M.R., Lashkari, D., Hollinshead, M., Roffman, J.L., Smoller, J.W., Zöllei, L., Polimeni, J.R., Fischl, B., Liu, H., Buckner, R.L., 2011. The organization of the human cerebral cortex estimated by intrinsic functional connectivity. J. Neurophysiol. 106 (3), 1125–1165.
Uddin, L.Q., 2015. Salience processing and insular cortical function and dysfunction. Nat. Rev. Neurosci. 16 (1), 55–61.
Uslu, O., Burhanoglu, B.B., Hinc, A.C., Gonul, A.S., 2025. Disrupted cortical organization in schizophrenia based on functional connectivity gradients. Eur. Arch. Psychiatry Clin. Neurosci. 5 (8), 1–8.
Vos de Wael, R., Benkarim, O., Paquola, C., Lariviere, S., Royer, J., Tavakol, S., Xu, T., Hong, S.-J., Langs, G., Valk, S., Misic, B., Milham, M., Margulies, D., Smallwood, J., Bernhardt, B.C., 2020. BrainSpace: a toolbox for the analysis of macroscale gradients in neuroimaging and connectomics datasets. Commun. Biol. 3 (1), 103.
Walther, S., Strik, W., 2012. Motor symptoms and schizophrenia. Neuropsychobiology 66 (2), 77–92.
Walton, E., Hibar, D.P., van Erp, T.G.M., Potkin, S.G., Roiz-Santiañez, R., Crespo-Facorro, B., Suarez-Pinilla, P., van Haren, N.E.M., de Zwarte, S.M.C., Kahn, R.S., Cahn, W., Doan, N.T., Jørgensen, K.N., Gurholt, T.P., Agartz, I., Andreassen, O.A., Westlye, L.T., Melle, I., Berg, A.O., Morch-Johnsen, L., Færden, A., Flyckt, L., Fatouros-Bergman, H., Jönsson, E.G., Hashimoto, R., Yamamori, H., Fukunaga, M., Jahanshad, N., De Rossi, P., Piras, F., Banaj, N., Spalletta, G., Gur, R.E., Gur, R.C., Wolf, D.H., Satterthwaite, T.D., Beard, L.M., Sommer, I.E., Koops, S., Gruber, O., Richter, A., Krämer, B., Kelly, S., Donohoe, G., McDonald, C., Cannon, D.M., Corvin, A., Gill, M., Di Giorgio, A., Bertolino, A., Lawrie, S., Nickson, T., Whalley, H. C., Neilson, E., Calhoun, V.D., Thompson, P.M., Turner, J.A., Ehrlich, S., 2018. Prefrontal cortical thinning links to negative symptoms in schizophrenia via the ENIGMA consortium. Psychol. Med. 48 (1), 82–94.
Wang, F., Yuan, T., Pereira Jr, A., Verkhratsky, A., Huang, J.H., 2016. Glial cells and synaptic plasticity. Neural Plast. 2016 (1), 5042902.
Wang, Y., Tang, W., Fan, X., Zhang, J., Geng, D., Jiang, K., Zhu, D., Song, Z., Xiao, Z., Liu, D., 2017. Resting-state functional connectivity changes within the default mode network and the salience network after antipsychotic treatment in early-phase schizophrenia. Neuropsychiatr. Dis. Treat. 13 (2), 397–406.
Wobrock, T., Guse, B., Cordes, J., Wölwer, W., Winterer, G., Gaebel, W., Langguth, B., Landgrebe, M., Eichhammer, P., Frank, E., Hajak, G., Ohmann, C., Verde, P.E., Rietschel, M., Ahmed, R., Honer, W.G., Malchow, B., Schneider-Axmann, T., Falkai, P., Hasan, A., 2015. Left prefrontal high-frequency repetitive transcranial magnetic stimulation for the treatment of schizophrenia with predominant negative symptoms: a sham-controlled, randomized multicenter trial. Biol. Psychiatry 77 (11), 979–988.
Xiang, J., Ma, C., Chen, X., Cheng, C., 2025. Investigating connectivity gradients in schizophrenia: integrating functional, structural, and genetic perspectives. Brain Sci. 179.
Xie, Y., Li, C., Guan, M., Zhang, T., Ma, C., Wang, Z., Ma, Z., Wang, H., Fang, P., 2024. The efficacy of low frequency repetitive transcial magnetic stimulation for treating auditory verbal hallucinations in schizophrenia: insights from functional gradient analyses. Heliyon 10 (9).
Yao, G., Luo, J., Li, J., Feng, K., Liu, P., Xu, Y., 2024. Functional gradient dysfunction in drug-naïve first-episode schizophrenia and its correlation with specific transcriptional patterns and treatment predictions. Psychol. Med. 54 (15), 4106–4118.
Yi, S., Wang, Q., Wang, W., Hong, C., Ren, Z., 2024. Efficacy of repetitive transcranial magnetic stimulation (rTMS) on negative symptoms and cognitive functioning in schizophrenia: an umbrella review of systematic reviews and meta-analyses. Psychiatry Res. 333 (3), 115728.